**ELSEVIER**

# Three-dimensional shape reconstruction of abdominal aortic aneurysm

Mun-Bo Shim, Murat Gunay, Kenji Shimada*

*Carnegie Mellon University, USA*

## Abstract

This paper presents an effective computational technique for reconstructing a three-dimensional shape of an abdominal aortic aneurysm (AAA), from a limited number of computed tomography (CT) images. The three-dimensional template geometry of a healthy abdominal aorta is used as *a priori* knowledge, and the template geometry is deformed by extended free-form deformation (EFFD), to generate a patient-specific AAA geometry. A two-step optimization scheme is devised to find an optimal set of EFFD parameters that match the cross-section of a deformed template with an AAA contour shown in a CT image. The geometric continuity of a deformed model is maintained by raising the order of the polynomial function used in EFFD. Experimental results show that the proposed method creates the three-dimensional shape of AAA suitable for structural finite element analysis and computational fluid dynamics for medical diagnosis.
© 2007 Elsevier Ltd. All rights reserved.

*Keywords:* Geometry reconstruction; Free-form deformation; Extended free-form deformation; Continuity control; Abdominal aortic aneurysm

## 1. Introduction

Abdominal aortic aneurysm (AAA), a degenerative disease, often causes the rupture of an arterial wall. Since such a rupture leads to a death in most cases, an accurate prediction of AAA rupture is critical. Although the maximum transversal diameter of AAA greater than a threshold value of 5 or 6 cm is most commonly used in clinical practice as a primary indicator of a near-future rupture, not all large aneurysms rupture. There is clinical evidence that small aneurysms can also rupture abruptly [18].

An AAA rupture is a biomechanical phenomenon. From a mechanical viewpoint, a rupture occurs when wall stresses exceed the maximum stress the tissue can withstand; therefore, biomechanical analysis can be used to assess the risk of a rupture of an aneurysm.

A patient-specific AAA geometry, obtained from tomographic images, is the foundation for a thorough biomechanical analysis of AAA to assess rupture risk, because maximum wall stress depends on the geometry of an aneurysm. Recently, patient-specific AAA geometry was generated using magnetic resonance imaging (MRI), and computed tomography (CT), computational fluid dynamics, structural analysis, and fluid–structure interaction have been performed successfully [10,18,24]. In these analyses however, generating the geometry is one of the most time-consuming processes, requiring a considerable amount of manual intervention.

In this study, an effective computational technique for reconstructing a three-dimensional model of AAA from a set of tomographic cross-sections is presented. The proposed method enables automatic reconstruction of a patient-specific AAA shape from a limited number of CT images. The three-dimensional template geometry of a healthy abdominal aorta is used as *a priori* information, and the template geometry is deformed by extended free-form deformation (EFFD). A two-step optimization scheme is devised to locate an optimal set of EFFD parameters that match the cross-section of a deformed template with an AAA contour, shown in a CT image. The geometric continuity of the deformed model is achieved by raising the order of the polynomial function used in EFFD.

The proposed method has two major advantages: (1) the method reconstructs a patient-specific three-dimensional shape quickly, automatically and robustly by using a template geometry, and (2) the method always generates a topologically and geometrically valid shape for structural finite element analyses and computational fluid dynamics for medical diagnosis.

* Corresponding address: Department of Mechanical Engineering, Carnegie Mellon University, 5000 Forbes Avenue, Pittsburgh, PA 15213, USA. Tel.: +1 412 268 3614; fax: +1 412 268 3348.

*E-mail address:* shimada@cmu.edu (K. Shimada).

Fig. 1. Two-dimensional error calculation.



(a) Input: template and CT contours   (b) Initial EFFD lattice   (c) Optimized EFFD lattice   (d) Smoothed geometry
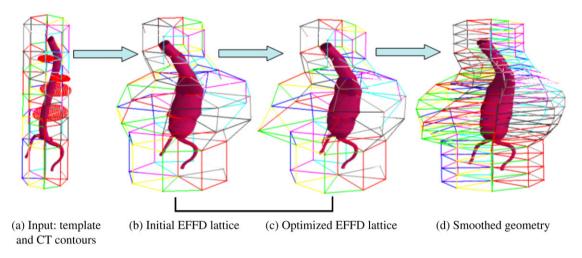
Fig. 2. Overview of the technical approach.

The rest of the paper is structured as follows: Previous approaches are discussed in Section 2. Section 3 presents the problem statement and the proposed technical approach. Section 4 elaborates on the proposed three-dimensional shape reconstruction method. Section 5 presents the results of applying the method to some test cases. Conclusions are given in Section 6.

## 2. Previous approaches

This section presents a survey of previous research on three-dimensional shape reconstruction from a set of CT images. They can be classified into two categories: methods without a deformable object and methods with a deformable object.

### 2.1. Shape reconstruction methods without a deformable object

Shape reconstruction methods without a deformable object can be further classified into two groups [9]: surface-based methods and volume-based methods.

In surface-based reconstruction, three fundamental problems must be addressed in order to build a surface between contours in adjacent cross-sections: correspondence, tiling and branching [1,19]. The correspondence problem involves finding the correct connections between the contours of adjacent CT images. If the spacing between CT images is large, it is difficult to determine the correct correspondence. The tiling process uses slice chords to triangulate a strip lying between two contours in adjacent CT images. It is difficult to find an optimal and topologically correct tiling. The branching problem occurs when a contour in one image may correspond to more than one contour in the adjacent CT image. A contour in one image, having no corresponding contour in the adjacent CT image, forms a hole, and the existence of branches significantly complicates the task of tiling.

Volume-based reconstruction is based on voxel, a spatial equivalent to pixel. Since CT images are arranged on a regular two-dimensional grid, it is natural to extend them to volume elements. The marching cubes algorithm is most popularly used in volume-based reconstruction [16]; it creates a polygonal representation of a boundary surface of an object from the voxel data.

Although the above two methods are popular in three-dimensional shape reconstruction research, they have several limitations. Surface-based reconstruction methods often cause a topologically and/or geometrically invalid shape with erroneous holes or overlapping surfaces. As a result, they usually require
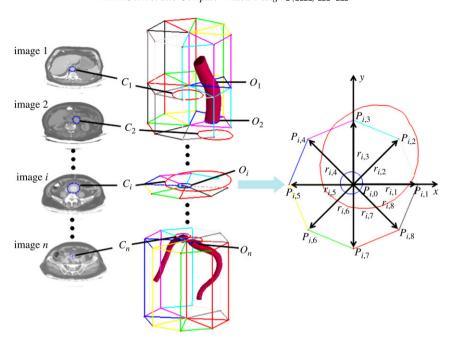
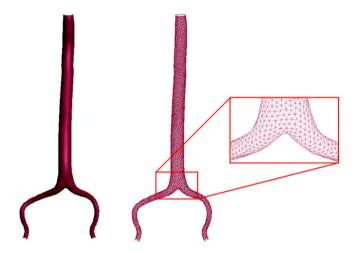Fig. 3. Control variables of extended free-form deformation lattice.



Fig. 4. Template geometry of an abdominal aorta used in the shape reconstruction.

a considerable amount of manual intervention to correct the errors. Volume-based reconstruction methods have a large volume of data to be manipulated. If the distance between an adjacent cross-section is too large compared to the pixel distance, an additional interpolation step is necessary to avoid jagged shapes.

## 2.2. Shape reconstruction methods with a deformable object

Shape reconstruction methods with a deformable object have been used to generate the geometrical model of an anatomical structure from medical images. The methods overcome many of the limitations of the shape reconstruction methods discussed in the previous section by providing a template of an object shape and by incorporating the knowledge of an anatomical structure. They are also capable of accommodating the significant variability of a biological structure over time and across different individuals. The use of a deformable object can result in a faster, more robust reconstruction technique that ensures a globally smooth and coherent surface.

In the last two decades, shape reconstruction techniques with a deformable object have been studied intensively [2–5, 7,8,12,13,15,20,21,25]. Among the first and primary uses of deformable objects in medical image analysis was a deformable contour, called "a snake" [13], to segment a structure in an image [8,15]. However, the application of a snake for extracting a region of interest has some limitations. Snakes work well only when an initial geometry is given near the target region of interest. The next formation of deformable objects for medical image analysis was a deformable surface. Miller et al. constructed a polygonal approximation of a sphere and geometrically deformed it until its surface conformed to a target object in CT images [20]. The reconstruction process is formulated as the minimization of a cost function where the desired behavior of the spherical object is determined by a local cost function associated with each vertex of the polygonal model. Battle et al. proposed the usage of a deformable object to reconstruct an unknown attenuation map of the torso from a set of transmission scans [3,4,7]. The deformable object tightly links the description of the object elements (for example, triangles) to the way it can be deformed. The reconstruction methods deform a triangular mesh by directly estimating the displacements of the triangle vertices; the number of the vertices of a geometrical object is $10^3$–$10^6$, or more. A number of researchers have incorporated the knowledge of a target object shape into a deformable object by using a deformable shape template. The use of anatomical knowledge to guide shape recovery is important for robust and automatic interpretation of medical images. Bardinet et al. fitted a deformable superquadric to segmented three-dimensional cardiac images and then refined the superquadric fit using a volumetric deformation technique known as free-

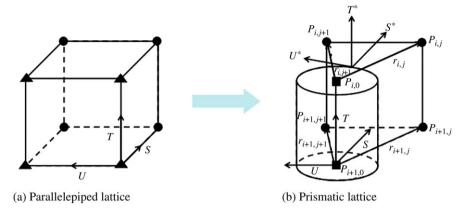(a) Parallelepiped lattice        (b) Prismatic lattice

Fig. 5. A prismatic lattice obtained by merging two pairs of points of a parallelepiped lattice: ● is an unchanged control point. ▲ is a control point to be merged. ■ is a merged control point.
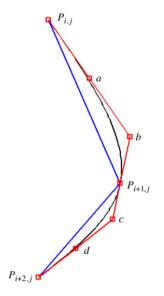


Fig. 6. Piecewise Bézier curves with $C^1$ continuity.

form deformation (FFD) [2]. Montagnat et al. proposed a general algorithm for performing shape reconstruction with a deformable object in a robust and accurate manner by using FFD and registration [21]. Battle et al. investigated the use of FFD to describe the continuous transformation of space to match a set of transmission measurements [5]. Gunay and Shimada proposed an x-ray based three-dimensional bone shape reconstruction by using hierarchical FFD [11,25].

Although FFD is a powerful tool in shape reconstruction methods with a deformable object, it has a few drawbacks. The deformation technique handles only a specific type of deformation, defined by a parallelepiped lattice [6]. The parallelepiped shape of the FFD lattice with a lower-order polynomial function allows only limited types of deformation. Although the range of deformation can be expanded by using a higher-order polynomial function, this leads to a greater number of design variables in optimization, making the process slow and unstable. Furthermore, when FFD is used to reconstruct three-dimensional geometry through the optimization process, there remains a large number of design variables; these often make the problem more complex, and additional information –

such as a regularizing term in the optimization criterion – may be required to solve the reconstruction problem [2].

## 3. Problem statement and technical approach

The problem of three-dimensional shape reconstruction of an abdominal aortic aneurysm (AAA) can be stated as follows: Given:

- CT images of an abdominal aortic aneurysm, and
- Three-dimensional template geometry of a healthy abdominal aorta

Generate:

Three-dimensional shape of the abdominal aortic aneurysm suitable for structural finite element analysis and computational fluid dynamics for medical diagnosis.

The reconstruction process finds the deformation that minimizes the distance between a CT scan contour and a cross-sectional contour of the deformed template model. According to the previous study, free-form deformation (FFD) can handle this problem [11,25]. The use of FFD in three-dimensional limb-bone geometry reconstruction is suitable because the cross-sectional shape of a limb-bone is relatively simple, and for orthopedic surgical planning the detailed cross-sectional shape is not necessary. However, when a cross-sectional shape is more complex, as in the case of AAA, an FFD-based method does not work well. In the current work, therefore, the use of extended free-form deformation (EFFD) is proposed.

The proposed technical approach to the AAA shape reconstruction problem is to find control lattice parameters of EFFD, or deformation parameters that minimize the distance between a CT scan contour and a cross-sectional contour of the deformed template model. The method also generates a topologically and geometrically valid shape for structural finite element analyses and computational fluid dynamics for medical diagnosis, by using three-dimensional template geometry of a healthy abdominal aorta as *a priori* knowledge.

As illustrated in Fig. 1, the distance between a CT scan contour, denoted as $C_i$, and a cross-sectional contour of the deformed template model, denoted as $O_i$, is measured by a two-dimensional error, denoted as $a_i$. This two-dimensional error is

(a) EFFD with a linear polynomial function.

(b) Generation of new control points by the natural cubic spline.
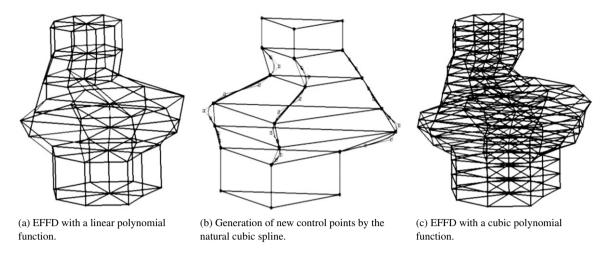
(c) EFFD with a cubic polynomial function.

Fig. 7. Extension of the deformation with a linear polynomial function to the deformation with a cubic polynomial function by the natural cubic spline.
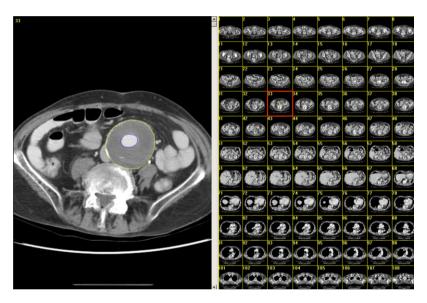


Fig. 8. Abdominal CT scans with outlined AAA contours.

used as the objective function of the optimization process. The two-dimensional bounding box that contains both a CT scan contour and a planar cross-sectional contour of the template model is created. This bounding box is then discretized to shoot rays and intersect with the contours. The line segments shown in Fig. 1 are summed up to compute an approximate distance between a CT scan contour and a cross-sectional contour of the deformed template model.

Fig. 2 shows an overview of our technical approach. The input consists of both the template geometry of a healthy abdominal aorta and a set of CT images whose contours are digitized manually. A cylindrical lattice is generated by assembling $8 \times 6$ prismatic cells, as shown in Fig. 2. The top and bottom planes of each layer of eight prismatic cells correspond to one CT image. The template geometry is then embedded inside the lattice as shown in Fig. 2(a). A two-step optimization consists of the generation of initial EFFD lattice and the optimization of EFFD parameters. In order to explain

the two-step optimization, assume there are $n$ CT images, which include contours $C_i$ for $i = 1, \ldots, n$, as shown in Fig. 3. A cross-sectional contour ($O_i$ for $i = 1, \ldots, n$) of the deformed template lies on the plane corresponding to each of the CT images.

First, the initial EFFD lattice is created by making the center of a cross-sectional contour of the deformed template model match that of a CT scan contour, by moving all of control points, $P_{i,j}$ for $j = 0, \ldots, 8$, simultaneously so that the center of gravity of $O_i$ matches that of $C_i$. Then, the positions of the two contours are roughly matched by finding an optimal radius, $r_{optimal}$, on the contour via one variable optimization (see Fig. 2(b)). This process is repeated through the entire plane. In the EFFD optimization, the distance between two contours is minimized by finding an optimal radius of each of the cells on a plane (see Fig. 2(c)). Although each of the optimal radii is obtained by one variable optimization, this process must be repeated for all cells on a plane because
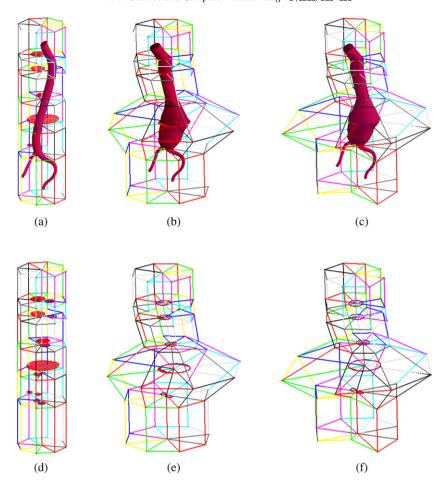
Fig. 9. Three-dimensional shape reconstruction of the external wall of AAA with EFFD: (a) initial shape, (b) shape from initial EFFD lattice, (c) shape from optimized EFFD lattice, (d) initial contour, (e) contour from initial EFFD lattice, and (f) contour from optimized EFFD lattice.
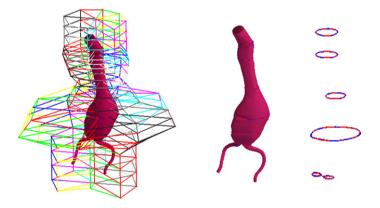


Fig. 10. Three-dimensional shape reconstruction of the external wall of AAA satisfied with $C^1$ continuity.

these radii are coupled variables in optimization. The whole process is repeated throughout the entire plane. Finally, the deformed model is refined and made smooth by applying the geometric continuity condition to the deformation lattice (see Fig. 2(d)).

## 4. Three-dimensional shape reconstruction

This section presents technical details of the proposed three-dimensional shape reconstruction method using: (1) three-dimensional template geometry of a healthy abdominal

aorta, (2) extended free-form deformation, and (3) geometric continuity control.

### 4.1. Three-dimensional template geometry of an abdominal aorta

Three-dimensional template geometry of an abdominal aorta, shown in Fig. 4, is used as a base model for reconstructing a patient-specific three-dimensional shape. The template is represented as a shell of a polygonal mesh, consisting of a set of vertices and a set of triangular faces. The triangular

Fig. 11. Verification of three-dimensional shape reconstruction of the external wall of AAA.



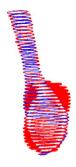(a) 10 CT images.    (b) 15 CT images.    (c) 20 CT images.

Fig. 13. Verification of three-dimensional shape reconstruction of the external wall of AAA.

boundary representation of the template makes it easy to calculate a planar cross-section. It is important that there be no gap or overlap between faces; any gap or overlap will make it impossible to create a quality mesh for structural finite element analyses and computational fluid dynamics for medical diagnosis. Moreover, the resolution of the template should be fine enough so that its shape features will remain after the template is deformed. Our current template polygonal model consists of 4433 vertices and 8823 triangular polygons.

## 4.2. Extended free-form deformation

EFFD used in this study is an extension of the FFD technique. This method uses non-parallelepiped three-dimensional lattice. We will present EFFD after the implementation of FFD is explained.

The basic idea of Sederberg's FFD [22] is that, rather than directly deforming the object, the object is embedded in a rectangular space that is then deformed. This technique defines a free-form deformation of space by specifying a trivariate Bézier solid, which acts on a parallelepiped region of space. One physical and intuitive analogy of FFD is that a flexible object is "molded" in a clear plastic block and the entire block is deformed by stretching, twisting, squeezing. As the block is deformed, an object trapped inside is accordingly deformed. The deformation is defined as follows:

(1) Impose a local coordinate system on a parallelepiped region of space by specifying any point $X$ in the following form
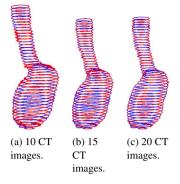
$$X = X_0 + sS + tT + uU, \tag{1}$$

where $S, T$, and $U$ are direction vectors, respectively. The coordinates, $s, t$, and $u$ are given by

$$(s, t, u) = \left( \frac{T \times U \cdot (X - X_0)}{T \times U \cdot S}, \frac{S \times U \cdot (X - X_0)}{S \times U \cdot T}, \right.$$
$$\left. \times \frac{S \times T \cdot (X - X_0)}{S \times T \cdot U} \right). \tag{2}$$

Note that $0 \le s \le 1, 0 \le t \le 1$, and $0 \le u \le 1$ for any interior point to the parallelepiped.

(2) Impose a grid of control points $P_{ijk}$ on the parallelepiped. Let $l, m$, and $n$ be the number of subdivisions along each of the three directions, $S, T$, and $U$. These form $l + 1$ planes in the $S$ direction, $m + 1$ planes in the $T$ direction, and $n + 1$ planes in the $U$ direction. These points lie on a lattice, and their locations are defined

$$P_{ijk} = X_0 + \frac{i}{l} S + \frac{j}{m} T + \frac{k}{n} U. \tag{3}$$

(3) Deform the control points on the parallelepiped into new control points.

(4) Reconstruct any point in three-dimensional space by first calculating its $(s, t, u)$ coordinates, and then applying these coordinates to the trivariate Bézier function

$$X_{ffd} = \sum_{i=0}^{l} \sum_{j=0}^{m} \sum_{k=0}^{n} B_l^i(s) B_m^j(t) B_n^k(u) P_{ijk} \tag{4}$$

with the Bernstein polynomials
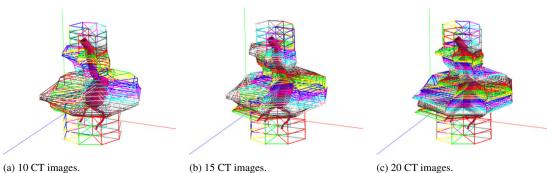
$$B_l^i(s) = \frac{l!}{i!(l-i)!} s^i (1-s)^{l-i}. \tag{5}$$



(a) 10 CT images.      (b) 15 CT images.      (c) 20 CT images.

Fig. 12. Three-dimensional shape reconstruction of the external wall of AAA satisfied with $C^1$ continuity.

FFD is a very useful modeling technique, but it is too restrictive to allow flexible deformation of an object. The restriction is mainly due to the shape of the lattice. The parallelepiped shape of the FFD lattice prohibits arbitrarily shaped deformation.

In contrast to FFD, extended free-form deformation (EFFD) allows arbitrarily-shaped deformation by using a non-parallelepiped lattice [6,17]. In the extension of FFD to EFFD, the primary difficulty is to calculate $(s, t, u)$ coordinates of the model points in a non-parallelepiped lattice. Coquillart used a Newton approximation to calculate the coordinate [6]. MacCracken and Joy presented a free-form deformation technique, which uses arbitrary lattices, namely, Catmull–Clark subdivision volumes [17]; but the lattice space definition is time consuming and difficult. Also, this technique requires a great deal of CPU time and memory.

A prismatic EFFD lattice is obtained by merging two pairs of control points of a parallelepiped lattice, as shown in Fig. 5 [6]. The method used in FFD can be applied to calculate the coordinates by using the projection method [26]. This projection method calculates the $(s, t, u)$ coordinates in a prismatic lattice as follows:

(1) Compute $t$ in the same way as FFD, while the $T^*$ axis is the cylinder axis.
(2) Define $S^*$ axis as the radial coordinate and $U^*$ axis as the angular coordinate on the base plane of the cylinder.
(3) Calculate $u$ from the angle between a point projected on the $S^*U^*$ plane and $S^*$ axis.
(4) The line which connects the origin with the mid-point of the others in the triangle can be defined. The projected point on the $S^*U^*$ plane is projected on the line again.
(5) Calculate $s$ from the ratio between the entire line length and the length obtained by the projected point.

### 4.3. Numerical optimization

In order to solve the two-step optimization problem, we use the sequential quadratic programming (SQP) algorithm [14, 23]. SQP is one of the most effective methods for solving optimization problems with significant nonlinearity. It is thus suitable for our reconstruction problem with the highly nonlinear cost function.

Feasible sequential quadratic programming (CFSQP) [14] is used in this study. This is an implementation in C of a modified version of SQP that generates feasible iterations.

### 4.4. Geometric continuity control

It is our considered decision to use a linear subdivision and interpolate it with a higher-order polynomial function later. When the prismatic lattice is deformed, the deformation maintains only the $C^0$ continuity, and the tangent continuity ($C^1$) between two cells is not guaranteed. Two ways for maintaining $C^1$ continuity are: (1) using a linear subdivision and raising the order of an interpolation function later; and (2) using a higher-order polynomial function from the beginning. We choose the former strategy because the deformation with a higher-order polynomial function leads to a greater number of
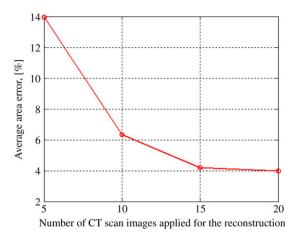


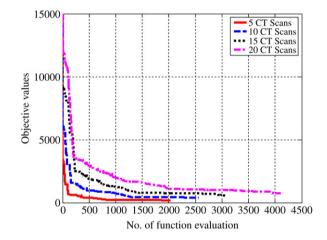Fig. 14. Effect of the number of CT images used for three-dimensional shape reconstruction.



Fig. 15. Convergence history of three-dimensional shape reconstruction of the external wall of AAA.
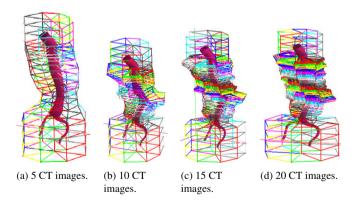


(a) 5 CT images.  (b) 10 CT images.  (c) 15 CT images.  (d) 20 CT images.

Fig. 16. Three-dimensional shape reconstruction of the lumen of AAA with $C^1$ continuity. The proposed method generates a more detailed and accurate AAA shape as the number of input cross-sectional images increases.

design variables in optimization, making the process slow and unstable.

It is possible to apply the deformations with a cubic polynomial function in a piecewise manner in order to maintain $C^1$ continuity between the lattices. For example, assuming that two cubic Bézier curves are connected, as shown in Fig. 6, the $C^1$ continuity is achieved by making $b$, $P_{i+1,j}$, and $c$ collinear.

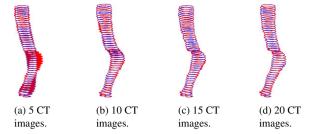(a) 5 CT images.  (b) 10 CT images.  (c) 15 CT images.  (d) 20 CT images.

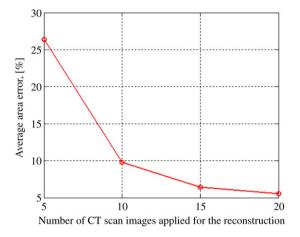Fig. 17. Verification of three-dimensional shape reconstruction of the lumen of AAA.



Fig. 18. Effect of the number of CT images used for three-dimensional shape reconstruction.

The deformation with a cubic polynomial function is obtained both by inserting two new control points between two control points in vertical direction and by interpolating all of the control points lying on the plane corresponding to a CT image. The natural cubic spline is used to make three control points around the common control point of the lattices collinear. Fig. 7 shows the refinement of an EFFD lattice with a linear polynomial function to a EFFD lattice with a cubic polynomial function by using the natural cubic spline.

## 5. Results and discussion

Some case studies have been performed to verify the effectiveness of the proposed approach. EFFD with geometric continuity control, described in the previous section, is used to reconstruct a patient-specific AAA geometry from a limited number of CT images. Generally, there are two important contours shown in a CT image of AAA: the external contour of AAA, or the external wall, and the internal contour of AAA, or the lumen. In these case studies, the internal contour and the external contour of AAA are extracted separately from CT images.

Abdominal CT images with a 5 mm interval in the axial direction were used, and the CT scans were imported into a commercial image processing software package, 3D Doctor v3.5, Able Software Corp., USA. The external and internal contours of the AAA were marked manually for each CT image of the AAA, as shown in Fig. 8. The z-coordinate of each image was added subsequently using the image interval information.
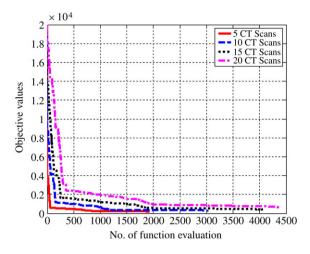


Fig. 19. Convergence history of three-dimensional shape reconstruction of the lumen of AAA.

Fig. 9 shows the entire process of reconstructing a three-dimensional shape of the external wall of AAA by using EFFD. Five of the contours (Fig. 8) thus created were first selected to recontruct the external wall of AAA. The initial position of three-dimensional template geometry of a healthy abdominal aorta was calibrated to be applied to the CT scan contours and the lattice size was initialized. In this study, the cylindrical lattice which came from eight prismatic cells were utilized on a CT image. The cells were layered according to the location of CT images, as shown in Fig. 9(a) and (d). Both the initial EFFD lattice and the optimized EFFD lattice were obtained through the two-step optimization explained in Section 3, as shown in Fig. 9(b), (e), (c) and (f). The $C^1$ continuity is obtained by refining the EFFD lattice with a linear polynomial function to an EFFD lattice with a cubic polynomial function, as shown in Fig. 10.

In order to verify the accuracy of the reconstructed shape, the average area error was investigated between the entire CT image contours and the cross-sectional contours of the deformed model corresponding to the CT image contours. The average area error was computed by:

$$\overline{AE} = \frac{1}{n} \sum_{i=1}^{n} \frac{a_i}{A_i} = \frac{1}{n} \sum_{i=1}^{n} \frac{1}{A_i} \sum_{j}^{m} l_{i,j} \Delta, \qquad (6)$$

where $m$ is the number of the line segments, $l_{i,j}$ the $j$th line segment on the $i$th CT image, and $\Delta$ spacing between the line segments. $a_i$, $A_i$ is the area error and the area of the $i$th CT image, as shown in Fig. 1. Fig. 11 shows the area error of the deformed model obtained by using five CT images. The average area error in this case is about 14%. In order to reduce the area error, we increased the number of CT images to 10, 15, and 20. Fig. 12 shows the deformed models obtained by applying EFFD with a cubic polynomial function. Again, the accuracy of the reconstructed shape was investigated by calculating the average area error, as shown in Fig. 13. Fig. 14 illustrates the effect of the number of CT images used for three-dimensional shape reconstruction on the accuracy of shape reconstruction. The more CT images are used, the more accurate the deformed

(a) healthy abdominal aorta        (b) exterior surface (c) interior surface
                                        of AAA          of AAA
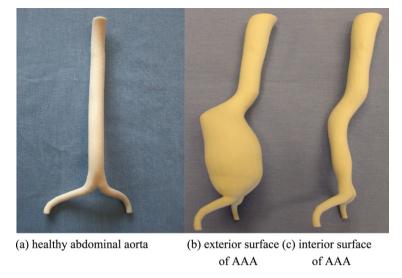
Fig. 20. Mockups of a healthy abdominal aorta and AAA.

model becomes. A patient-specific three-dimensional shape with less than 5% error can be obtained by using 15 CT images. This level of error is usually small enough for the purposes of medical diagnosis.

The converging history and computational time were investigated in order to evaluate the performance of EFFD. Fig. 15 shows the converging process of the external wall of an AAA obtained with 5, 10, 15, 20 CT images; it took 169, 267, 464, and 669 s, respectively to reach a converged result, using an AMD Athlon 1.83 GHz with 1.0 GB of memory. In Fig. 16, the convergence trend was steep in the initial EFFD process and steady in the EFFD optimization process, the reason being that in the initial EFFD process the distance between two contours was rapidly fitted by locating an optimal radius on each image via one variable optimization. In the EFFD optimization process, the distance between two contours was stably and steadily reduced, by numerical optimization repeated through all the cells on each image, because these radii are coupled variables. Moreover, it meant that when the prismatic lattice was deformed, the proposed method – which used a linear subdivision and raised the order of an interpolation function later – was reasonable.

For the lumen, (the internal contour of AAA), the same reconstruction process was performed with the contours obtained in Fig. 8. Fig. 16 shows the deformed models obtained by applying EFFD with a cubic polynomial function. The accuracy of the deformed models was investigated by calculating the average area error, as shown in Fig. 17. Fig. 18 explains the effect of the number of CT images used for three-dimensional shape reconstruction. The results obtained for the lumen are quite similar to the results from the external wall. To evaluate the performance of EFFD in the case of the lumen, the converging history and computational time were also investigated. The convergence trend and the computational time of the lumen were virtually identical to those of the external wall, as shown in Fig. 19.

As a means for verification of the reconstructed result, half-sized mockups of the interior and exterior surfaces of AAA were generated by using a commercial rapid prototyping machine (ZPrinter 310 System, Z corporation, USA), as shown in Fig. 20.

## 6. Conclusion

An effective computational technique was developed for reconstructing a three-dimensional shape of AAA from a limited number of CT scan images. The three-dimensional template geometry of a healthy abdominal aorta was used as a template, and the template geometry was deformed by EFFD to generate a patient-specific AAA geometry. A two-step optimization scheme was devised to find an optimal set of EFFD parameters that match a cross-section of deformed template with an AAA contour shown in a CT image. The geometric continuity of a deformed model was maintained by raising the order of the polynomial function used in EFFD.

Experimental results were presented to demonstrate the effectiveness of this method. The proposed method can reconstruct a patient-specific three-dimensional shape quickly, automatically, and consistently by using the template geometry after a set of contours from CT images are given. Both the template geometry and EFFD with a cubic polynomial function always generated a topologically and geometrically valid shape for structural finite element analysis and computational fluid dynamics for medical diagnosis.

# References

[1] Bajaj CL, Coyle EJ, Lin K-N. Arbitrary topology shape reconstruction from planar cross sections. Grap Models Image Process 1996;58(6): 524–43.

[2] Bardinet E, Cohen LD, Ayache N. A parametric deformable model to fit unstructured 3d data. INRIA, Tech. Rep. 2617. 1995.

[3] Battle XL, Cunningham GS, Hanson KM. Tomographic reconstruction using 3D deformable models. Phys Med Biol 1998;43:983–90.

[4] Battle XL, Cunningham GS, Hanson KM. 3D tomographic reconstruction using geometrical models. Proc SPIE 1997;3034:346–57.

[5] Battle XL, Le Rest C, Turzo A, Bizais Y. Three-dimensional attenuation map reconstruction using geometrical models and free-form deformations. IEEE Trans Med Imaging 2000;19(5):404–11.

[6] Coquillart S. Extended free-form deformation: A sculpturing tool for 3D geometric modeling. ACM SIGGRAPH Comput Graph 1990;24(4): 187–96.

[7] Cunningham GS, Hanson KM, Battle XL. Three-dimensional reconstructions from low-count SPECT data using deformable models. Opt Express 1998;2(6):227–36.

[8] Davatziko CA, Prince JL. An active contour model for mapping the cortex. IEEE Trans Med Imaging 1995;14(1):65–80.

[9] Elvins TT. A survey of algorithms for volume visualization. Comput Graph 1992;26(3):194–201.

[10] Finol EA, Keyhani K, Amon CH. The effect of asymmetry in abdominal aortic aneurysms under physiologically realistic pulsatile flow conditions. J Biomech Eng 2003;127:207–17.

[11] Gunay M. Three-dimensional bone geometry reconstruction from x-ray images using hierarchical free-form deformation and non-linear optimization. Ph.D. thesis. Carnegie Mellon University; 2003.

[12] Hanson KM, Cunningham GS, Jennings Jr GR, Wolf DR. Tomographic reconstruction based on flexible geometric models. In: Proc IEEE int conf on image processing, vol. II. 1994. p. 145–7.

[13] Kass M, Witkin A, Terzopoulos D. Snakes: Active contour models. Int J Comput Vis 1988;1(4):321–31.

[14] Lawrance C. et al. User's guide for CFSQP version 2.3: A C Code for solving (LargeScale) constrained nonlinear (minimax) optimization problems, generating iterates satisfying all inequality constrains. College Park (MD, USA): Electrical Engineering Department and Institute for Systems Research, University of Maryland; 1994.

[15] Lobregt S, Viergever MA. A discrete dynamic contour model. IEEE Trans Med Imaging 1995;14(1):12–24.

[16] Lorensen W, Cline H. Marching cubes: A high resolution 3D surface construction algorithm. Comput Graph 1987;21:163–9.

[17] MacCracken R, Joy KI. Free-form deformations with lattices of arbitrary topology. Comput Graph 1996;181–8.

[18] Di Martino ES, Guadagni G, Fumero A, Ballerini G, Spirito R, Biglioli P, et al. Fluid-structure interaction within realistic three-dimensional models of the aneurysmatic aorta as a guidance to assess the risk of rupture of the aneurysm. Med Eng Phys 2001;23:647–55.

[19] Meyers D. Reconstruction of surfaces from planar contours. Ph.D. thesis. University of Washington; 1994.

[20] Miller JV, Breen DE, Lorensen WE, O'Bara RM, Wozny MJ. Geometrically deformed models: A method for extracting closed geometric models from volume data. Comput Graph 1991;25(4): 217–226.

[21] Montagnat J, Delingette H. Globally constrained deformable models for 3D object reconstruction. Signal Processing 1997;71(2):173–86.

[22] Sederberg TW, Parry SR. Free-form deformation of solid geometric models. In: SIGGRAPH'86 proceedings. 1986. p. 151–60.

[23] Vanderplaats GN. Numerical optimization technqiues for engineering design. New York: McGraw Hill; 1984.

[24] Venkatasubramaniam AK, Fagan MJ, Mehta T, Mylankal KJ, Ray B, Kuhan G, et al. A comparative study of aortic wall stress using finite element analysis for ruptured and non-ruptured abdominal aortic aneurysms. Eur J Vasc Endovasc Surg 2004;28:168–76.

[25] Shimada K, Krause K, Mendicino R, Weiss L, Kanade T. Computer-aided bone distraction. US patent, US6.701.174. 2004.

[26] http://www.cse.ucsc.edu/classes/cmps260/Winter03/proj/yx51866/projectReport.html.